Modal Test and Parameter Updating of Metal Laser Sintered Components

Joseph D. Schoneman[1] **and Matthew S. Allen**[2]

[1] Graduate Student; e-mail: schoneman@wisc.edu

[2] Assistant Professor; e-mail: matt.allen@wisc.edu

University of Wisconsin — Department of Engineering Physics

1500 Engineering Drive

Madison, WI 53706

Abstract

Recent advances in additive manufacturing technology have made feasible the use of materials such as titanium and high-temperature nickel alloys in the construction of complex parts intended for production through techniques such as direct laser melting or direct laser sintering. These parts can be manufactured at a level of quality suitable not only for prototyping, but even for use as flight hardware. However, the evaluation of material properties is a challenge; melted metals will not retain the same properties as an equivalent cast metal, and factors such as part geometry, print density, and any post-processing techniques used will all influence the material properties of a given component. This paper uses modal analysis to update the isotropic material properties of metal components which are representative of flight hardware within the subsystems of a liquid rocket motor. Two different materials are examined: Ti 64 titanium alloy and INCONEL 718 nickel alloy.

Keywords: 3D Printing, Modal Test, Model Updating

1 INTRODUCTION

The advent and spread of additive manufacturing (AM) technologies, such as fused deposition modeling (FDM), selective laser sintering (SLS) or direct metal laser sintering/melting (DMLS/DMLM) — commonly referred to as *3D printing*[1] — has been met with rapid adoption in many areas of the aerospace industry. AM techniques are best applied to components which feature complex design features, low production runs, optimization for light weight, and exotic material requirements. Such requirements are prevalent in the aerospace industry in general, and the launch industry in particular. In the subfield of liquid rocket motor design, additively manufactured designs can make use of superalloys that would be either impossible or prohibitively expensive to manufacture using conventional casting or machining techniques.

A major area of interest related to AM technology is the estimation or validation of material properties of the built components. Depending on the manufacturing technique and material in question, the material may be extruded into a wire or powdered prior to the build; during the build process, either a laser or heated extruder head melts or lays down material in a layer-by-layer process which eventually builds up the full component. The various mechanical operations and phase changes which the

[1] Under some definitions, "3D printing" refers specifically to the manufacture of plastic parts, though it is often used as a catch-all term for any sort of additive manufacturing process. Here, the abbreviation "AM" is used to encompass all possible additive processes, and the more specific "DMLS" abbreviation is used to refer to the specific process in use for this paper.

material is subjected to may lead to significant changes from tabulated mechanical properties. Further, the layer-by-layer build process leads to the potential for orthotropic material properties which depend on build orientation.

Key elastic properties of a material can be evaluated through the use of the static tensile test; most significantly, the elastic modulus E, yield stress σ_y, ultimate stress σ_u, and Poisson's ratio ν. Biaxial testing can be used to identify the elastic constants of an anisotropic material. However, only specifically constructed test billets can be used on a tensile testing machine; tensile testing of operational components is not possible.

AM build processes admit the possibility of property variations between different component designs. First, since AM processes all rely on the heating and cooling of the build material, different components will feature different patterns of residual stresses. Perhaps more significant is the common use of "skin and core" construction[1], as shown in Figure 1. The outer skin of the structure is built at full density, often to a thickness of 1-3 mm, to maintain strength on the outer surface of the part. To save weight and material costs, the interior of the part is built at a reduced density. This is a useful design technique, but complicates the task of identifying accurate mechanical properties for a given material.

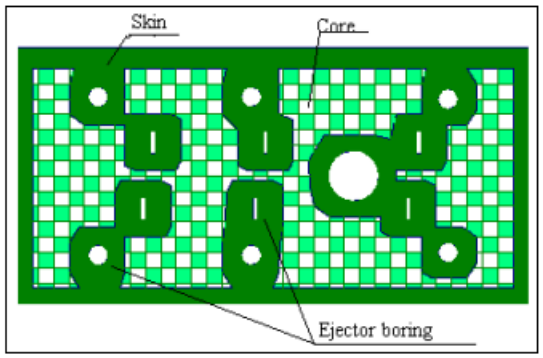

Figure 1: *Demonstration of the "skin & core" construction technique commonly used in AM processes[1]. The skin of the structure is built at full density, often to a thickness of 1-3 mm, while the inner core is built at reduced density to save weight and cost.*

As an alternative to static tensile testing, modal testing allows the recovery of natural frequencies and mode shapes of a component. From these, relevant material properties and physical dimensions can be inferred. Compared to static tensile testing, modal testing has several disadvantages when used to determine the material properties of a specific part:

- The material properties are only *estimated*, not observed. Estimation of the actual material properties requires a suitable model — usually a finite element model — which itself may be subject to error.
- The natural frequencies of a structure depend on both the density and elasticity of its material; if the density cannot be estimated, then accurate estimation of both parameters is difficult.
- Dimensional variations in the structure affect the natural frequencies and mode shapes independently of the material properties.
- No estimates of yield strength or ultimate strength can be made from a modal test.

However, several key advantages are apparent as well:

- Modal testing serves as a method to validate a finite element model as a whole — large discrepancies in frequencies or mode shapes can be found and rectified.
- Modal testing recovers the damping characteristics of the component, which heavily influence the design requirements for several types of dynamic loading and are difficult to compute in general.

- Modal testing is non-destructive and can be used on any component. Unlike tensile tests, modal tests do not require specialized geometry.

With these factors in mind, a modal test was conducted in conjunction with Orbital Technologies Corporation (ORBITEC); a propulsion and spacecraft systems company located in Madison, WI. In order to evaluate the accuracy and capabilities of AM techniques for the construction of propulsion components, ORBITEC commissioned a set of test articles from GPI Prototyping, Inc; an AM vendor located in Rockford, IL. The test components are shown in Figure 2; no surface finish was specified beyond the removal of support material. The print direction was from top to bottom as pictured in Figure 2. Two materials were evaluated: Titanium - 6% Aluminum - 4% Vanadium alloy (Ti 64) and an INCONEL 718 (INCO) nickel "superalloy."

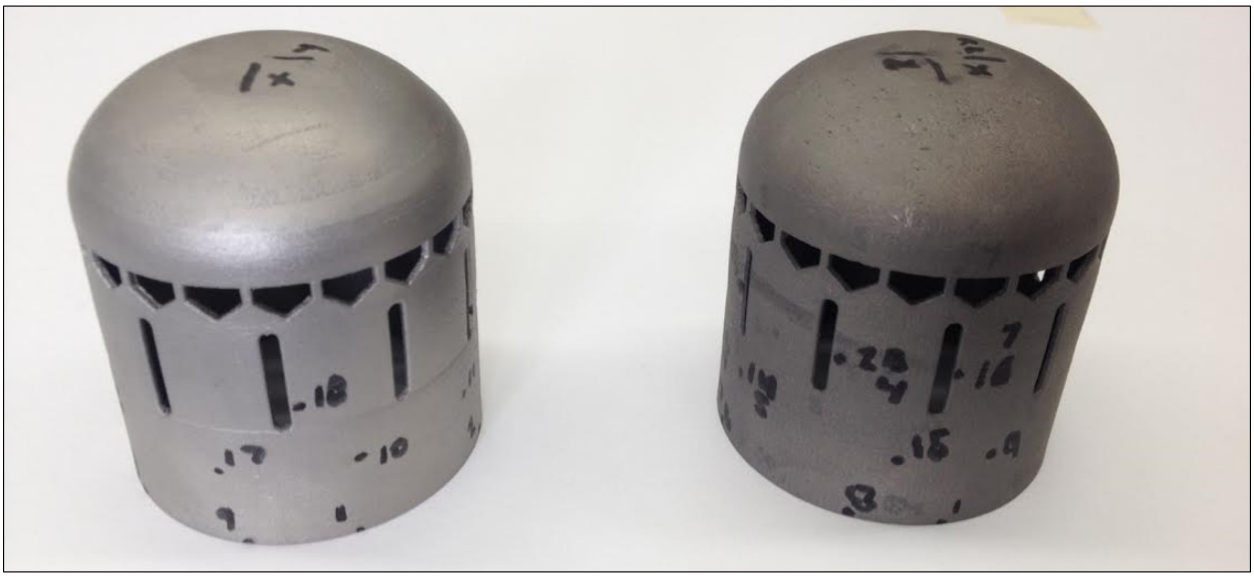

Figure 2: *INCO 718 (left) and Ti 64 (right) test components manufactured using the DMLS (Direct Metal Laser Sintering) process.*

Nominal mechanical properties for each material are shown in Table 1[2] [3].

Material	Elastic Modulus [$\mathrm{lb}/\mathrm{in}^2$]	Density [$\mathrm{slug}/\mathrm{in}^3$]
INCO 718	$29,000$	$7.62 \cdot 10^{-4}$
Ti 64	$16,000$	$4.12 \cdot 10^{-4}$

Table 1: *Nominal material properties used for initial finite element analysis.*

The remainder of this paper describes the construction of a finite element model, test procedures, and the parameter update procedure used to evaluate these components.

2 FINITE ELEMENT MODEL DEVELOPMENT

The use of a modal test to estimate material properties is dependent on the presence of a representative structural model, either analytical or numerical. For all but the most trivial of structures, analytical models are not feasible and instead the finite element method (FEM) is used to obtain the natural frequencies and mode shapes. In this case, Abaqus® finite element (FE) software was used for the analysis. Geometry from SolidWorks® modeling software can be directly imported into Abaqus as a

deformable solid. Once this is accomplished, a mesh is applied to the geometry.

Several meshing approaches are available. Tetrahedral elements can be used to mesh a solid of arbitrary shape at the cost of significantly increased element count, since the four-vertex tetrahedron does not fill nearly as much space as a six-vertex hexahedron. Hexahedral meshes, on the other hand, allow for much smaller element counts but almost always require significant geometric simplification of the component. Finally, a shell mesh applied to thin geometries is much more efficient and accurate than a mesh of solid elements over a thin cross section. Each of these approaches was evaluated for this geometry as follows:

- The full geometric complexity of the model was retained and a quadratic tetrahedral mesh (C3D10 elements in Abaqus) was applied.
- All filleted edges were removed in SolidWorks prior to import and a quadratic hexahedral mesh (C3D20) was applied to the entire model.
- Using the non-fillet geometry, a linear hexahedral mesh (C3D8) was applied to the "dome" area of the part, and "solid shell" elements (SC8R) were applied to the remainder of the component. "Solid shell" elements use a shell formulation, but inherit their thickness directly from the thickness of the solid geometry which they are applied to. The linear hexahedral mesh was required for element compatibility.

In the third case, a reduced integration formulation was examined to counteract the expected stiffness resulting from linear quadratic elements, but was found to provide overly soft results relative to the other two methods.

To evaluate the convergence properties of each mesh, three separate modal analyses using different refinement levels for each mesh type were performed. INCO 718 material properties were used for the convergence study. For initial analysis, isotropic elastic behavior was used, on the assumption that any anisotropic material would be evident in the test results. Table 2 and Figure 3 show the mesh parameters and results. Due to the near-symmetric configuration of the component, the first six modes appear as pairs of close natural frequencies; the lower of each frequency pair is reported as the 1st/3rd/5th frequency in Table 2. All of these are "flapping" modes of various orders, with the free edges of the cylinder predominant in the response. A three-dimensional view of the first mode pair is shown in Figure 4, while top-down views of the first ten modes of the INCO 718 structure (those of the Ti64 component are comparable) are depicted in Appendix A.

Type	DOF Count	Total Time [s]	Memory [MB]	$f_1[Hz]$	f_3 [Hz]	f_5 [Hz]
Quad. Tet. - Coarse	542859	101	6111	1453	3689	6637
Quad. Tet. - Medium	832059	261	9838	1452	3686	6631
Quad. Tet. - Fine	1948953	1924	25575	1450	3680	6617
Quad. Hex. - Coarse	195351	70	2348	1451	3681	6618
Quad. Hex. - Medium	450000	214	5948	1450	3677	6604
Quad. Hex. - Fine	1706199	7305	26776	1448	3674	6591
Lin. Hex + Shell - Coarse	32940	5	316	1461	3618	3684
Lin. Hex + Shell - Medium	83502	16	781	1455	3684	6618
Lin. Hex + Shell - Fine	246642	52	2366	1451	3676	6600

Table 2: *Mesh characteristics and frequency results of FEM convergence study. All listed frequencies correspond to "flapping modes" of different orders.*

Note that the finest refinements of the solid meshes both exceeded the 12 GB installed RAM of the workstation, leading to drastically longer computational time requirements incurred by read/write to the hard disk. Furthermore, the sensor placement procedure used below requires that the Abaqus results be imported into MATLAB, which places further restrictions on the largest model that can be accommodated. Examination of the results reveals that the "medium" refinement level of the solid/shell predicted only a slightly higher first natural frequency than the solid mesh counterparts, and was midway between the tetrahedral and hexahedral results for the third and fifth frequencies. As such, this was the model selected for import into MATLAB for sensor set selection.

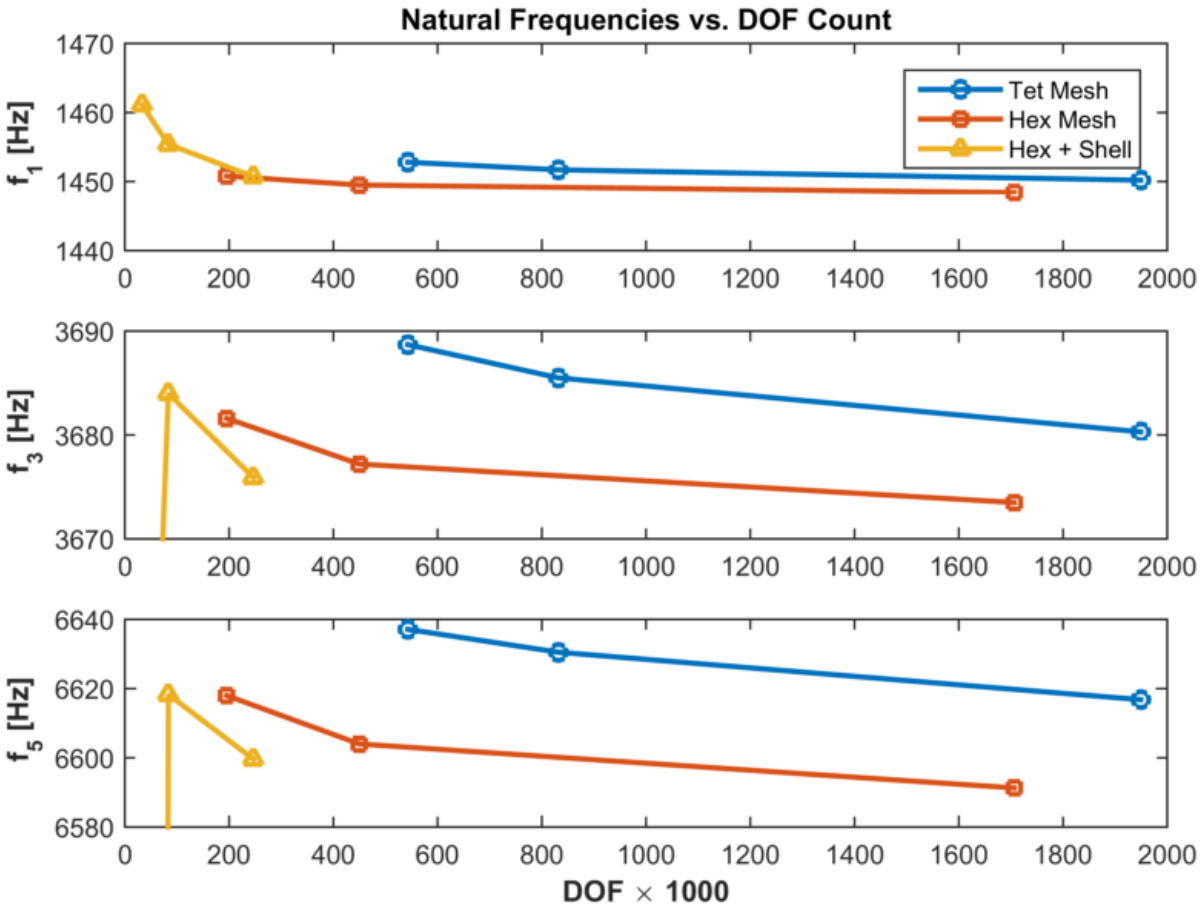

Figure 3: *Visual depiction of the convergence study results.*

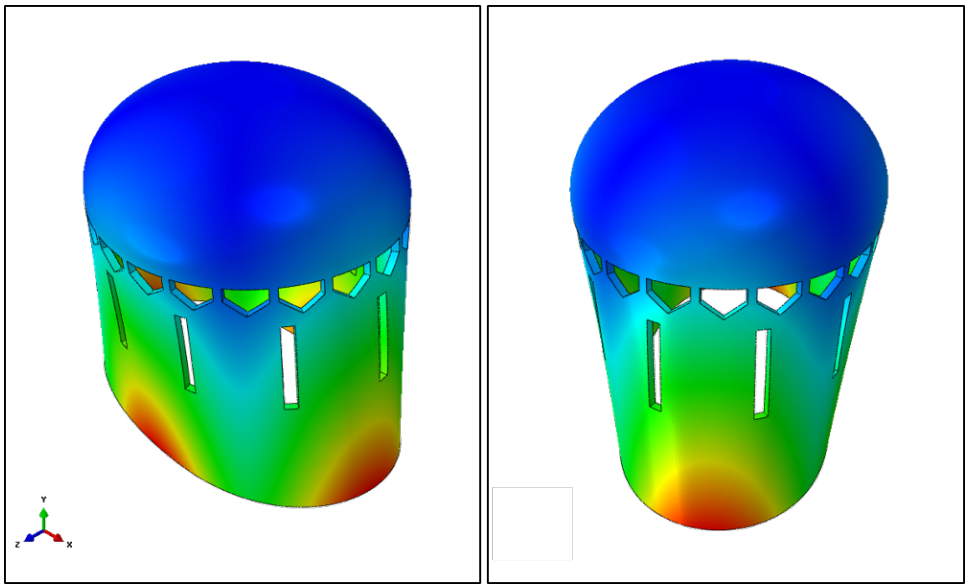

Figure 4: *Three dimensional view of the one/two mode pair; contours depict modal deformation levels.*

A “truth” model for later comparison to experimental results was also selected. In this case, a balance between frequency convergence and model size led to selection of the medium hexahedral mesh; the finest refinement of this mesh showed only a marginal downward shift in frequency relative to the moderate level, at a greatly increased computation time.

3 MODAL TEST SETUP

Once the prototype parts were fabricated, the modal test was performed. The test method used was a roving hammer impact test. A four-channel data acquisition unit was available; three accelerometers were used as references. The components were tested in a free-free suspended condition; Figure 5 shows the articles instrumented for testing.

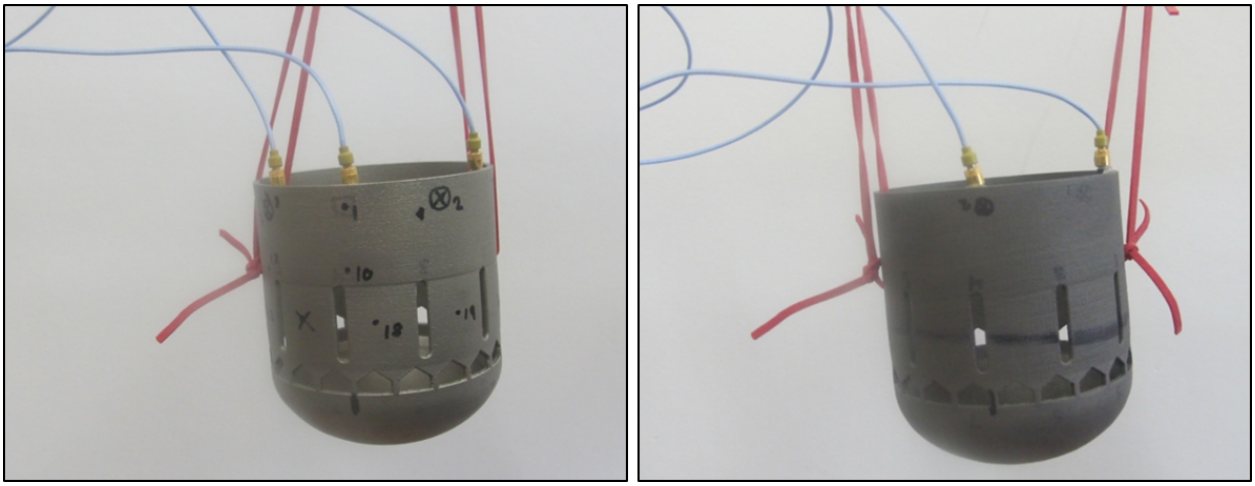

Figure 5: *INCO 718 (left) and Ti 64 (right) articles during the test procedure.*

Bruel & Kjaer software was used to monitor the input/output and compute compute accelerance frequency response functions for each impact point. Different sample frequencies and time windows were used for the Ti 64 and INCO 718 parts; a larger frequency range was used for the titanium version to attempt measurement of higher modes, while a closer frequency spacing was used for the Inconel version to better distinguish the closely spaced modes. Table 3 gives the acquisition settings for each test case. At each impact location, three signal averages were used to determine the frequency response function (FRFs) corresponding to that point.

Component	Frequency Range	Frequency Interval
Ti 64	20 kHz	3.1 Hz
INCO 718	10 kHz	1.56 Hz

Table 3: *Acquisition properties for each test case.*

While only three accelerometer channels were available, an arbitrary number of hammer excitation points could be selected. Increasing the number of impact points increases the resolution of the mode shapes, but the set of modes that can be identified is limited by the reference (accelerometer) locations. To select both the accelerometer and impact locations, the method of “Effective Independence” was used [4]. This technique seeks to maximize the Fisher Information Matrix $\mathbf{Q}$ of a structure, defined as

$$\mathbf{Q} = \mathbf{\Phi}^T \mathbf{\Phi} \tag{1}$$

where Φ is the target modal matrix of the structure at each reference location. For the INCO component, the target mode set included the first six modes; for the titanium structure, the first ten. There are multiple methods to place sensors and actuators using Effective Independence. In this case, an "additive" technique starting from a single accelerometer location was used[5]. Since the accelerometers and impact locations act in the radial direction on the structure, rather than the Cartesian coordinate system used in the finite element program, the FE mode shapes were transformed to a cylindrical coordinate prior to sensor selection. Only the external radial locations were included in the possible set of locations. Three accelerometer/impact locations and 21 impact-only locations were selected, for a total of 24 impact locations. Figure 6 shows the resulting impact and accelerometer locations for each version of the part.

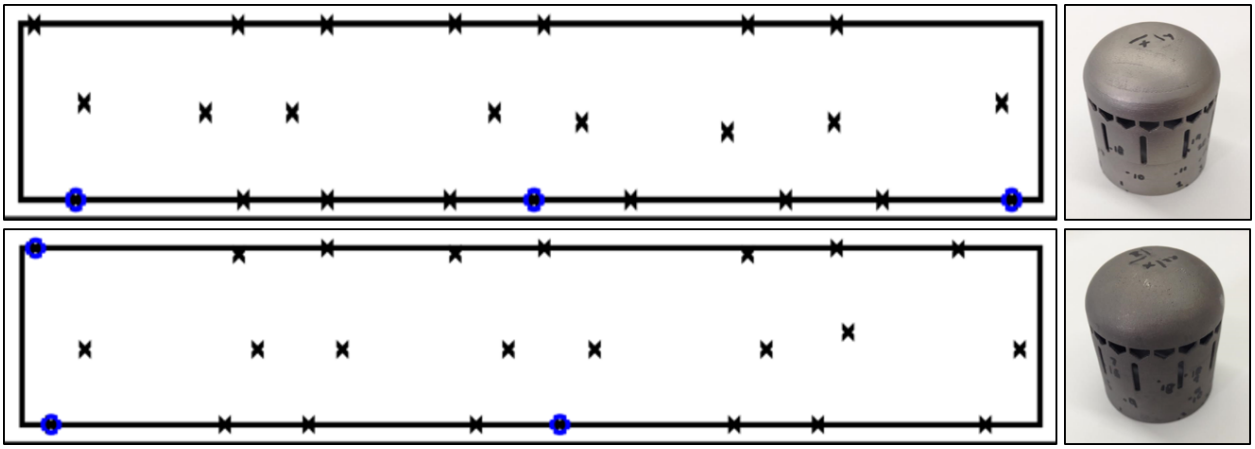

Figure 6: *Hammer impact (black crosses) and accelerometer (blue circles) locations for each part. Top: INCO 718 component. Bottom: Ti 64 component.*

With the test complete and FRFs obtained, an implementation of the algorithm of mode isolation (AMI)[6] was used to obtain each component's modal parameters. The implementation in question is a a multi-input multi-output method using a single degree-of-freedom linear least squares fit, with the option to use a multi-degree-of-freedom linear least squares fit in the presence of close or repeated modes. The resulting natural frequencies and critical damping ratios identified for each component are presented in Table 4, while the measured FRF envelope and estimated curve fit FRF is shown in Figure 7. The modal assurance criterion (MAC) matrices of the test results are shown in Figure 8.

	INCO 718				Ti 64			
Mode	FEM Freq [Hz]	Test Freq [Hz]	Pct. Error	ζ [%]	FEM Freq [Hz]	Test Freq	Pct Error	ζ [%]
1	1448	1361	6.44	0.43	1487	1474	0.93	0.45
2	1451	1367	6.16	0.25	1487	1482	0.32	0.32
3	3673	3420	7.40	0.25	3773	3715	1.57	0.36
4	3678	3431	7.19	0.28	3773	3734	1.03	0.34
5	6590	6111	7.84	0.29	6776	6598	2.69	0.93
6	6595	6131	7.57	0.47	6776	6623	2.31	0.71
7	–	–	–	–	8988	8712	3.17	0.85
8	–	–	–	–	8991	8831	1.81	0.50
9	–	–	–	–	9807	9987	-1.81	0.36
10	–	–	–	–	9957	10014	-0.57	0.56

Table 4: *Modal test results for both components.*

The INCO 718 test results are clearly superior to those from the Ti 64 component. The titanium was a more difficult material

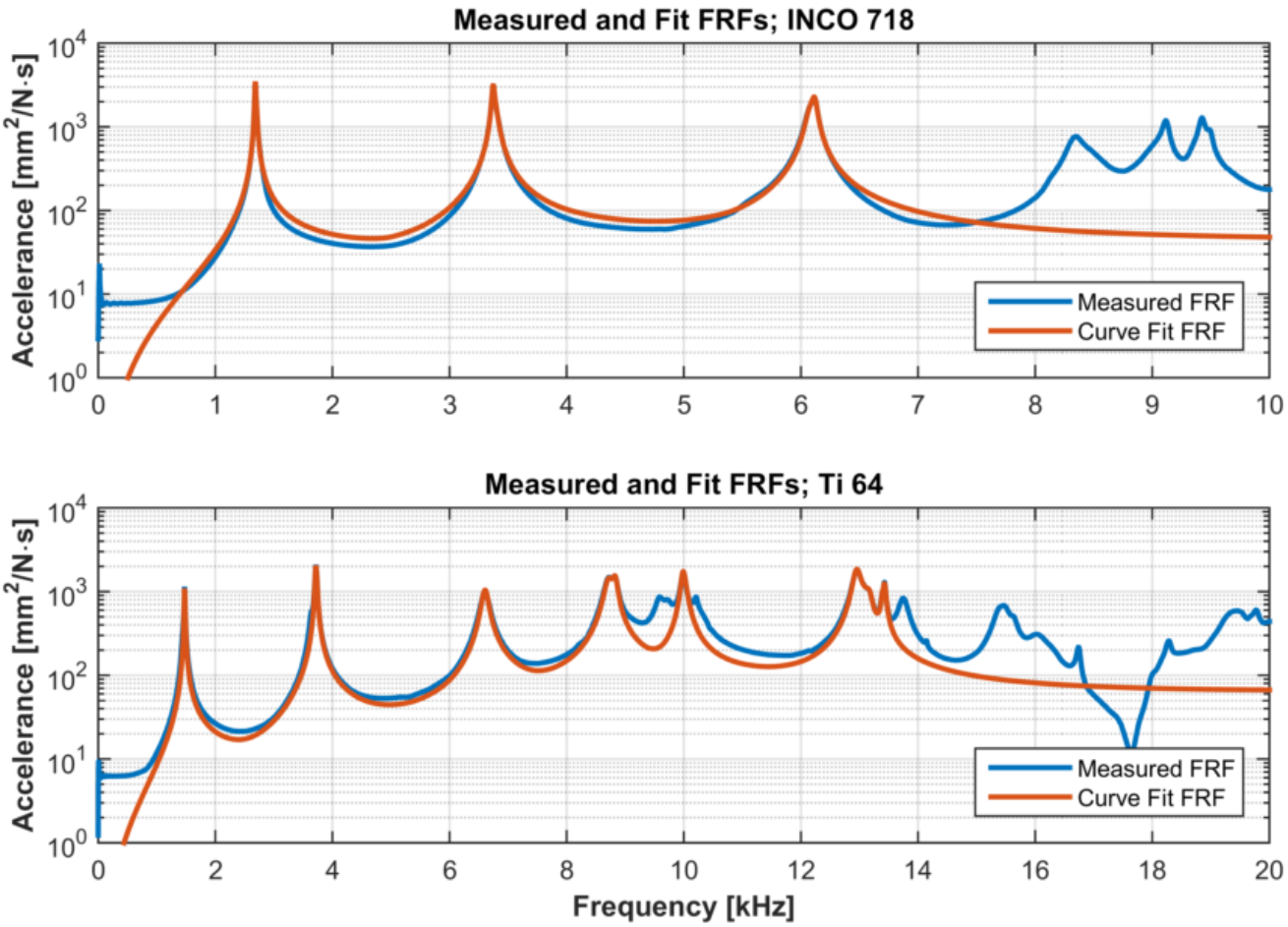

Figure 7: *Measured and estimated composite FRFs of each component.*

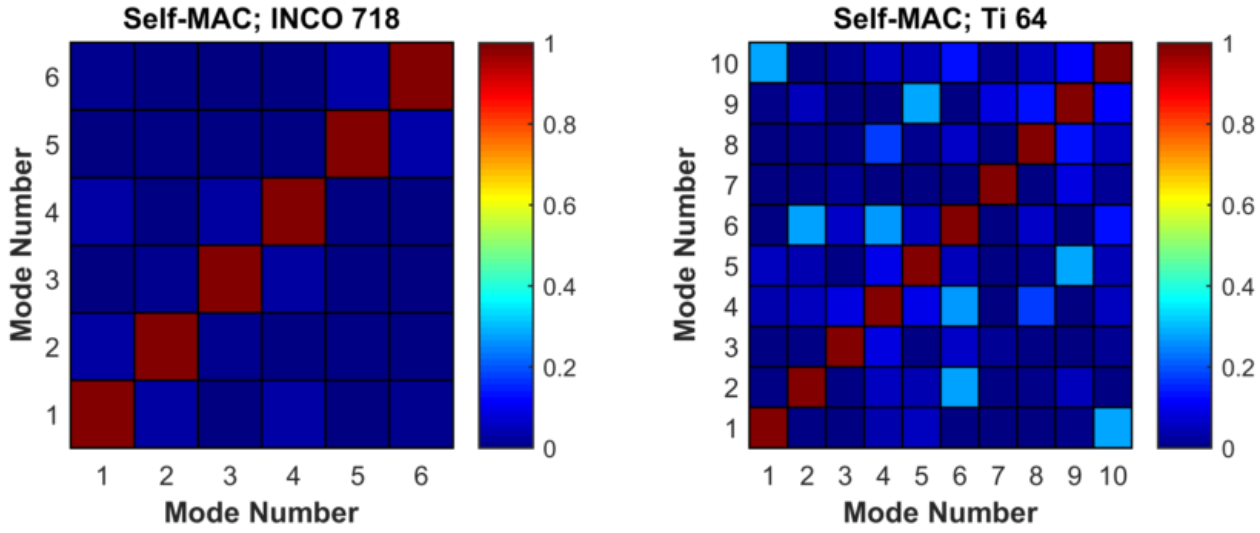

Figure 8: *Self-MACs of the test results for each component.*

on which to obtain clean hammer impacts due to the lighter weight of the component. Any clear "double-hits" were ignored and re-tested, but the overall quality of the Ti 64 measurements was lower than those from the INCO part.

4 PARAMETER UPDATE PROCEDURE

With a numerical model and set of test result in hand, the final task is to use these values to estimate each material's density and modulus of elasticity. In general, model updating requires an optimization framework linked to a full finite element code. Commercial software packages, such as ATA Attune™, are also available to perform model correlation procedures.

In this case, frequency errors are already quite low and all modes seem to be in error by similar amounts, suggesting acceptable results can be achieved by assuming isotropic material properties and concentrating on the ratio of density to modulus of elasticity. Given the size of these components, their actual densities can be estimated as well. Based on the minimum and maximum feasible values of measured density, upper and lower bounds on the modulus of elasticity can be formed.

4.1 Density Estimation

The weight of each component is easily measured with high accuracy, but a volume estimate was more difficult to obtain. The volume of water displaced by each item was measured in a 2.75 inch diameter test tube, however, the total displacement levels were small and sensitive to measurement errors. Two sets of marks were made for each displacement measurement; the averages of these two distances were used as upper and lower bounds on component volume. Finally, maximum and minimum density values were estimated by dividing the largest possible mass by the smallest possible volume and vice versa. Table 5 summarizes the density estimation measurements and results for each material.

	INCO 718	Ti 64
Mass [g]	110.05 ± 0.01	61.07 ± 0.01
Volume [in^3]	$8.249 \cdot 10^{-1} \pm 1.262 \cdot 10^{-2}$	$8.382 \cdot 10^{-1} \pm 2.227 \cdot 10^{-3}$
Density [$\mathrm{slug}/\mathrm{in}^3$]	$7.621 \cdot 10^{-4} \pm 1.173 \cdot 10^{-5}$	$4.161 \cdot 10^{-4} \pm 1.037 \cdot 10^{-6}$

Table 5: *Mass and volume measurements for each component along with the resulting estimated density values.*

4.2 Least-Square Parameter Fit

With an available value for material density, the natural frequencies are assumed to be functions of the elastic modulus only. A least-squares approach involving only the natural frequencies can be used to infer the values of this material property. From common analytical expressions for the natural frequencies of other types of structures, the i^{th} natural frequency of this component is assumed to take the form

$$f_i = \sqrt{\frac{E}{\rho}}\alpha_i \tag{2}$$

where α_i is a value which depends on the geometry of the structure and the modeshape in question. To estimate the actual elastic modulus, set up a least-squares minimization problem in E:

$$\min_{E} \quad \mathbf{y}(E)^T\mathbf{y}(E) \tag{3}$$

where the vector $\mathbf{y} = \dfrac{\mathbf{f}_{FE}^2(E) - \mathbf{f}_t^2}{\mathbf{f}_t^2}$ is an error vector written in terms of the finite element frequencies $\mathbf{f}_{FE}(E)$ and test frequen-

cies $\mathbf{f}_t$; the exponent and division symbols are understood to refer to "elementwise" operations. Re-writing in terms of Equation 2 leads to

$$y_i = \frac{E_{FE}}{E_t}\frac{\rho_t}{\rho_{FE}}\left(\frac{\alpha_{FE}}{\alpha_t}\right)_i^2 - 1 \tag{4}$$

for the i^{th} element of $\mathbf{y}$. The "FE" subcript refers to nominal properties used to compute the natural frequencies, while the "t" subscripts refer to actual properties of the test article. The density ρ_t has been estimated for each component, so only E_t remains to be found. Re-write Equation 4 by setting $x = \frac{E_{FE}}{E_t}$ and $\beta_i = \frac{\rho_t}{\rho_{FE}}\left(\frac{\alpha_{FE}}{\alpha_t}\right)_i^2$ so that $y_i = x\beta_i - 1$. The least-squares problem is solved by finding an x such that

$$\nabla \mathbf{y}^T(x)\mathbf{y}(x) = 0 \tag{5}$$

Since only a single optimization variable is in use, each element of $\nabla \mathbf{y}(x)$ is simply $\frac{\partial y_i(x)}{\partial x} = \beta_i$ and x can be found from

$$x = \frac{\sum_i \beta_i}{\sum_i \beta_i^2} \tag{6}$$

Finally, β_i can be written in terms of the known test frequencies, finite element frequencies, and density ratio as

$$\beta_i = \frac{\rho_t}{\rho_{FE}}\left(\frac{f_t}{f_{FE}}\right)_i^2 \tag{7}$$

where ρ_{FE} is the "nominal" material value from Table 1 and ρ_t, with its associated upper and lower bounds, is the estimated density value from Table 5. Once x is found, the modulus of elasticity is estimated using

$$E_t = xE_{FE} \tag{8}$$

4.3 Estimation Results

In principle, the procedure above can be performed iteratively through the finite element program, but a single pass of the calculation proved sufficient to provide acceptable results. The updated elastic modulus and density value for each component, along with upper and lower bounds, are shown in Table 6.

	INCO 718		Ti 64	
	Value	Percent of Nominal	Value	Percent of Nominal
Density [$\mathrm{slug/in^3}$]	$7.62 \cdot 10^{-4} \pm 1.17 \cdot 10^{-5}$	100.07 ± 1.54	$4.23 \cdot 10^{-4} \pm 6.54 \cdot 10^{-6}$	102.68 ± 1.59
Elastic Modulus [$\mathrm{lb/in^2}$]	$2.53 \cdot 10^{7} \pm 3.90 \cdot 10^{5}$	87.27 ± 1.34	$1.59 \cdot 10^{7} \pm 2.46 \cdot 10^{5}$	99.27 ± 1.54

Table 6: *Updated parameter estimation results from the frequency-only least squares minimization technique.*

The finite element models were re-analyazed in Abaqus using these values; resulting frequencies for the INCO 718 component are shown in Table 7, those for the Ti 64 component are shown in Table 8.

	Frequencies [Hz]			Error [%]	
Mode	FEA - Nominal	Test	FEA - Updated	Nominal	Updated
1	1448	1361	1358	6.44	-0.18
2	1451	1367	1358	6.16	-0.65
3	3673	3420	3446	7.40	0.75
4	3678	3431	3446	7.19	0.42
5	6590	6111	6188	7.84	1.27
6	6595	6131	6189	7.57	0.94

Table 7: Updated natural frequency results for the INCO 718 component.

	Frequencies [Hz]			Error [%]	
Mode	FEA - Nominal	Test	FEA - Updated	Nominal	Updated
1	1487	1474	1454	0.93	-1.36
2	1487	1482	1454	0.32	-1.95
3	3773	3715	3687	1.57	-0.73
4	3773	3734	3688	1.03	-1.26
5	6776	6598	6622	2.69	0.37
6	6776	6623	6623	2.31	-0.00
7	8988	8712	8785	3.17	0.83
8	8991	8831	8787	1.81	-0.50
9	9807	9987	9585	-1.81	-4.03
10	9957	10014	9732	-0.57	-2.82

Table 8: Updated natural frequency results for the Ti 64 component.

5 CONCLUSION

A modal test and frequency-only model update procedure was performed for metal parts manufactured using the DMLS process. Two materials, INCO 718 and Ti 64, were examined.

Test results from the INCO 718 component showed a uniform overestimation of the first six natural frequencies by roughly 6-8%. Damping ratios between 0.2% and 0.5% were observed for these modes. Based on the uniformity of the frequency error, an isotropic parameter update procedure was used, together with a measured estimate of the density, to obtain on updated value of the elastic modulus as 87.3% of the nominal value of 29 KSI. Post-update, the maximum frequency error fell to 1.3% for mode 5, with all other frequency errors below 1%.

The Ti 64 component showed much less departure from its nominal elastic modulus, with a maximum error of 3.2% between test and nominal FEA results. Damping ratios between 0.3% and 1.0% were measured for the first ten modes of the titanium article. The update procedure yielded a modulus of elasticity at 99.3% of nominal from a comparison of the first ten natural frequencies. Post-update frequencies were in some cases worse than their nominal counterparts, with modes 9 and 10 increasing and their respective errors of -4.0% and -2.8% the largest magnitude present. All other errors were below 2% in absolute value.

Orthotropic effects may have influenced the Ti 64 component to some extent, but were not observable for the first six modes of the INCO component. For this particular configuration, the measured modes all involved motions featuring predominantly axial stretching, making it difficult to observe the effects of anisotropy. Additionally, the thin-walled construction seems to have avoided any significant level of variable-density material in the structure, as seen from the measured values of density for each material.

As additive manufacturing techniques continue to gain prominence, modal testing techniques will continue to be an important part of the model validation toolbox. Additive techniques allow for complex designs featuring variable density, minimum use of material, and complex integral features; the ability to validate material properties on a component basis is critical to designing durable and efficient structures for future aerospace applications. As a non-destructive test method applicable to nearly any structure, modal tests will play a key role in enabling these capabilities.

ACKNOWLEDGMENTS

This material is based upon work supported by the National Science Foundation Graduate Research Fellowship under Grant No. DGE-1256259. Any opinion, findings, and conclusions or recommendations expressed in this material are those of the authors(s) and do not necessarily reflect the views of the National Science Foundation.

References

[1] Electro Optical Systems GmbH, *Design Rules for DMLS*.

[2] Special Metals, *INCONEL alloy 718*, 2007.

[3] Electro Optical Systems GmbH, *Material Data Sheet, EOS Titanium 64*, October 2011.

[4] D. C. Kammer, "Sensor placement for on-orbit modal identification and correlation of large space structures," *Journal of Guidance, Control, and Dynamics*, vol. 14, no. 2, pp. 251–259.

[5] D. C. Kammer, "Sensor set expansion for modal vibration testing," *Mechanical Systems and Signal Processing*, vol. 19, no. 4, pp. 700–713.

[6] M. S. Allen and J. H. Ginsberg, "A global, single-input multi-output (simo) implementation of the algorithm of mode isolation and application to analytical and experimental data," *Mechanical Systems and Signal Processing*, vol. 20, no. 5, pp. 1090–1111.

APPENDIX A

The first ten mode shapes and frequencies of the INCO 718 component obtained from a finite element analysis are shown in Figure 9. A top-down viewpoint is used, and only the lowermost nodes in the structure are included. All of the modes are "flapping modes" of various order, and all but modes nine and ten occur as pairs of "close" natural frequencies.

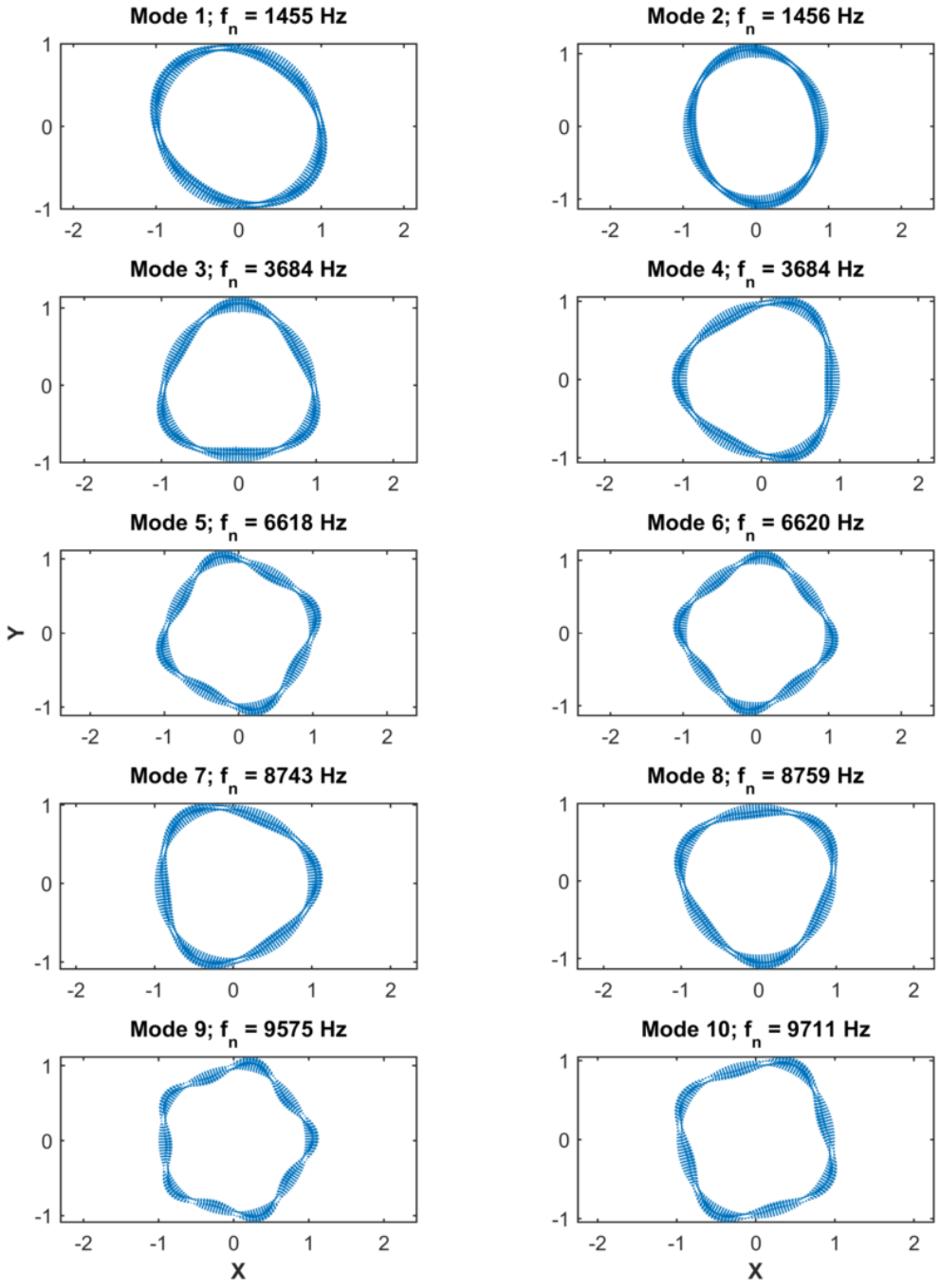

Figure 9: *Mode shapes and frequencies of the INCO 718 component, shown from a top-down view. Only the lowermost nodes are included in these images.*